

Ordinary Hall anomaly due to the Fermi surface shape in MnAs

C. Helman^{1,*}, A. M. Llois², and M. Tortarolo²

¹*Centro Atómico Bariloche, Comisión Nacional de Energía Atómica, S. C. de Bariloche, CP8400, Pcia de Rio Negro, Argentina*

²*Instituto de Nanociencia y Nanotecnología, CONICET-CNEA. Centro Atómico Constituyentes, Avenida General Paz 1499, B1650 Villa Maipú, Buenos Aires, Argentina*



(Received 21 May 2021; accepted 19 October 2021; published 8 November 2021)

We analyze the influence of the Fermi surface (FS) shape on magnetotransport properties, particularly on the Hall effect in the MnAs compound. Evidence of opposite conduction polarities for different crystal directions (*goniopolarity*) and a strong dependence of carrier type has been observed in MnAs films with an applied magnetic field. To understand this behavior, we developed a semiclassical model together with the Boltzmann transport theory that takes into account both the applied magnetic field and the FS shape. The MnAs FS is obtained by means of density functional theory, showing a clear dominance of the hyperboloid shape. Our study corroborates that the specific topology of the Fermi surface gives rise to a *goniopolar* behavior in the Hall transport. These theoretical results are supported by magnetotransport measurements on MnAs thin layers epitaxially grown on GaAs(001) and on GaAs(111), allowing us to explore the transport characteristics for two different crystal directions of the system.

DOI: [10.1103/PhysRevB.104.195109](https://doi.org/10.1103/PhysRevB.104.195109)

I. INTRODUCTION

The shape of the Fermi surface (FS) has been used to describe transport properties since the early days of materials science. Pioneering works by Pippard [1] and Lifshitz [2] theoretically prove that the magnetotransport behavior depends on the type of orbits that the wave vector performs in momentum space. These orbits are classified as open or closed within the characteristic time τ between two scattering events. The magnetoresistance (MR) and especially the Hall resistivity present different behaviors with the magnetic field depending on the type of orbit. Closed orbits lead to a linear dependence of the Hall resistivity and a saturating MR with increasing applied magnetic field. If the closed orbits on the FS enclose a region with lower energy, then positive values are expected for the Hall resistivity (hole type) and negative values in the opposite case (electron type). On the other hand, open orbits lead to a quadratic dependence of the Hall resistivity (hole type) and to a nonsaturating magnetoresistance with applied magnetic field.

The above-mentioned behavior of closed/open orbits in momentum space is well reproduced when modeling the FS using ellipsoids connected with a neck through the boundaries of the Brillouin zone (BZ) [1,3,4]. Other attempts to describe the magnetotransport properties use a tubularlike FS model, but this kind of analysis emphasizes more on the connectivity of the surface than on the concavity [1,5]. Recently, He *et al.* [6] showed that the concavity of the FS leads to simultaneous electron- and holelike magnetotransport properties, especially when presenting open orbits. Hence, for different crystal directions, the transport properties present opposite conduction

polarities. This effect, denoted *goniopolar* by the authors, was theoretically and experimentally studied for NiSn₂As₂ [6–8]. The origin of this phenomenon is straightforward in the case of a one band FS when it is singly connected with open orbits in one crystal direction and closed orbits in another direction. The different kinds of orbits give rise to a noticeable different behavior in electron transport measurements for different crystal directions [9]. In the case of the Hall effect (HE), the *goniopolarity* is manifested when the ordinary Hall coefficient R_H presents the opposite sign when measuring it for different crystal orientations as a function of the applied magnetic field. Similar behavior is also observed in the case of the Seebeck effect when the thermopower has the opposite sign for different crystalline orientations [6].

Manganese arsenide (MnAs) is a good candidate to be classified as a *goniopolar* material because it presents simultaneously electron- and holelike transport behavior, as earlier observed by Berry *et al.* [10]. Their MR and the HE measurements in MnAs/GaAs(001) epilayers reveal the presence of both electron and holes in the magnetotransport, with a contribution that varies with temperature and magnetic field. Also, Friedland *et al.* [11] observed mainly the same characteristics in the magnetotransport measurements done on MnAs/GaAs, finding that the carrier type strongly depends on crystal orientation: the MnAs/GaAs(001) samples exhibit mixed holelike and electronlike conductivity already at zero magnetic field, while in the case of MnAs/GaAs(111) the low-temperature transport is dominated by holes at zero magnetic field.

To explain their results the authors of Ref. [10] propose a two carrier model, while in Ref. [11] a model based on spherical bands with a small number of impurities [12] is used. Nowadays, we know that MnAs shows a complex Fermi surface, topologically different from those of spherical models and the good quality of the MnAs/GaAs epilayers

*christianhelman@cnea.gov.ar

[13–15] diminishes the role of impurities and domains for low-temperature transport phenomena.

In this work, we analyze the magnetotransport properties of MnAs from both experimental and theoretical points of view. In Sec. II we present the necessary theoretical background to explain our transport results. Then in Sec. III A we describe MnAs using the *ab initio* calculations and present the FSs from which we modeled the magnetotransport behavior, and in Sec. III B our measurements (MR, HE, and magnetization) on MnAs/GaAs for different crystal orientations are presented. Section IV offers a discussion on the theoretical model presented and on its accuracy to describe the experimental results.

II. THEORETICAL BACKGROUND

In order to describe the transport behavior in the presence of a magnetic field we restrict ourselves to a semiclassical treatment, in which the electrons can be thought of as classical particles obeying Fermi-Dirac statistics. At low temperature the features of the FS rule the electronic properties of metals, where the mean free time τ can be assumed to be large and only band dependent. This low temperature regime can be achieved in our theoretical approach by letting the smearing of the FS occupation function go to zero in the Boltzmann transport equation. Under these conditions the solution for the conductivity within the relaxation time approximation (RTA) is given by [16]

$$\sigma_{i,j} = e^2 \sum_n \tau^{(n)} \int_{FS^{(n)}} v_i^{(n)}(\mathbf{k}) \bar{v}_j^{(n)}(\mathbf{k}) \frac{dS}{|\nabla \varepsilon^{(n)}(\mathbf{k})|}, \quad (1)$$

where i, j are the Cartesian coordinates referred to as the crystal axis, e is the electron charge, and $\tau^{(n)}$ is the band dependent relaxation time. The index n indicates the band number, while the sum is over the bands that cross the Fermi level. The factor $1/|\nabla \varepsilon^{(n)}(\mathbf{k})|$ is related to the density of states of the n th band at the Fermi energy E_F . The integral over the FS of the n th band ($FS^{(n)}$) is obtained demanding that $\varepsilon^{(n)}(\mathbf{k}) = E_F$.

The integrand of Eq. (1) involves a product of two different kinds of velocities: $\mathbf{v}^{(n)}(\mathbf{k})$ is the gradient in momentum space of the energy band, and $\bar{\mathbf{v}}^{(n)}$ is defined as the weighted average over the past history of the charge carrier,

$$\bar{\mathbf{v}}_j^{(n)} = \int_{-\infty}^0 \frac{e^{t/\tau^{(n)}}}{\tau^{(n)}} v_j^{(n)}[\mathbf{k}(t)] dt. \quad (2)$$

$\mathbf{k}(t)$ is the group velocity and its time evolution in momentum space due to an applied magnetic field, (\mathbf{H}), is derived from the semiclassical set of equations and assuming no band crossing,

$$\mathbf{v}^{(n)} = \frac{1}{\hbar} \nabla_{\mathbf{k}} \varepsilon^{(n)}(\mathbf{k}), \quad (3a)$$

$$\hbar \dot{\mathbf{k}}(t) = -\frac{e}{c} \mathbf{v}^{(n)}[\mathbf{k}(t)] \times \mathbf{H}, \quad (3b)$$

$$\mathbf{k}(t=0) = \mathbf{k}_0 \in FS^{(n)}. \quad (3c)$$

Note that the set of Eq. (3) must be solved for each band that crosses the Fermi level and its solutions have to be inserted in Eq. (2). While $\mathbf{v}^{(n)}$ only depends on the wave vector \mathbf{k} , $\bar{\mathbf{v}}^{(n)}$ depends on both \mathbf{k} and on the magnetic field \mathbf{H} .

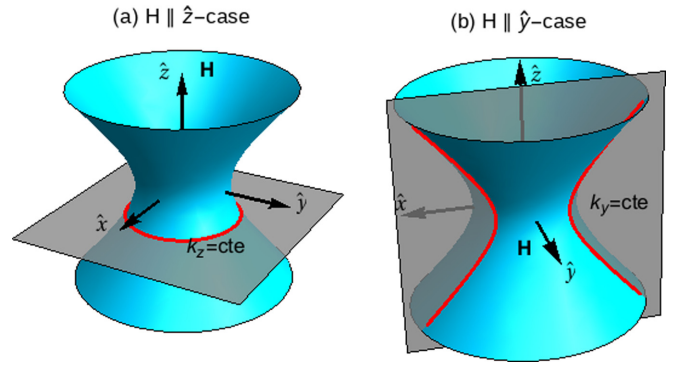


FIG. 1. Hyperboloid of revolution as a FS model from Eq. (4). The applied magnetic field is perpendicular to the gray planes and the intersection with FS is in red. (a) $\mathbf{H} \parallel \hat{z}$, only close orbits are possible. (b) $\mathbf{H} \parallel \hat{y}$, open orbits are allowed.

Two conservation laws can be derived from Eq. (3): (i) the wave vector trajectory in momentum space is given by the intersection of the FS with a plane perpendicular to the magnetic field direction (Fig. 1), and (ii) the energy remains constant in the presence of an applied magnetic field. Both conservation laws allow us to draw a preliminary picture of the results that can be expected for different FSs.

The resistivity tensor is obtained from $\rho = \sigma^{-1}$, which in principle requires a detailed description of σ . However, if we take into account the crystal symmetries of the compound together with Onsager's relation [$\rho_{i,j}(\mathbf{H}) = \rho_{j,i}(-\mathbf{H})$], then the interrelation among tensor components reduces the number of calculations required to obtain σ [17].

Hyperboloid Fermi surface

Many semiclassical transport calculations have been done considering spherical-like Fermi surfaces, with or without open orbits [1–4,9,16]. In this section we analyze the case of a FS that is concave in one direction and convex in other one. More precisely, a one sheet circular hyperboloid or an hyperboloid of revolution, which leads to noticeably different behavior for the conductance (or resistivity), as we discuss next.

Assume a FS given by

$$\varepsilon(\mathbf{k}) = \frac{\hbar^2}{2} \left(\frac{k_x^2}{m_x} + \frac{k_y^2}{m_y} - \frac{k_z^2}{m_z} \right) = E_F, \quad (4)$$

where m_i are the effective masses. The minus sign on the k_z^2 term indicates that the rotation symmetry axis is parallel to the z axis, while $m_x = m_y$ is the condition to have a hyperboloid of revolution. For our further analysis it is convenient to define the quantity $\alpha = \frac{m_z}{m_x}$ that is always a real positive number. If $\alpha \gg 1$, the hyperboloidal surface approaches a cylinder with a small concave curvature, while for $\alpha \approx 0$, the surface has two parabolic sheets joined by a narrow neck. In order to require the energy to reach perpendicularly the Brillouin zone boundaries, we can define energy as a continuous and piece-wise function. However, the change in the energy function from convex to concave is very small and its effect on the orbits is negligible [6].

In order to obtain $\bar{\mathbf{v}}^{(n)}$, we need the time-dependent wave-vector expression $\mathbf{k}(t)$, which describes the orbits on the FS. Since the z axis is an axis of rotational symmetry, only two cases are important to analyze: one where the magnetic field \mathbf{H} is parallel to the z axis, $\mathbf{H} \parallel z$ axis, and the other one when \mathbf{H} lies in the hexagonal planes, i.e., $\mathbf{H} \parallel y$ axis. The aforementioned conservation law can help us to have an insight of the solution Eq. (3). For the $H \parallel z$ case, the obtained orbits are closed circles, as shown in Fig. 1(a), where the time dependent solution has the characteristic frequency $\omega_z = \frac{eH}{cm_x}$. Instead, for the $H \parallel y$ case, the orbits are open hyperboloids, as shown in Fig. 1(b), with characteristic frequency $\omega_y = \frac{eH}{cm_x\sqrt{\alpha}} = \omega_z/\sqrt{\alpha}$. For simplicity we use $\omega_{z,y}$ instead of magnetic field \mathbf{H} . In the case of closed orbits, the physical meaning of ω is that (ii) goes like the inverse of the time to do one cycle, hence for higher magnetic field the more cycles the wave vector can complete. A similar concept can be drawn in the case of open orbits: a larger length of the orbit in the extended BZ is associated with an increasing magnetic field. In our approach, the RTA and low field condition can be fulfilled when $\omega\tau < 1$, which is the main difference with previous works like Refs. [1,2] and more recently [5], where the high field limit ($\omega\tau \gg 1$) is analyzed.

The expression of $\bar{\mathbf{v}}^{(n)}$ depends on the value of $\omega\tau$, the effective mass m_x , the mass parameter α , and the initial position of the wave vector \mathbf{k}_0 , which could be any point on the FS as pointed out in Eq. (3c). In order to obtain the final expression for the conductivity we must integrate over the FS. In this process the vector \mathbf{k}_0 becomes an integration variable and the final expression takes into account the history of all possible orbits on the FS.

The resistivity tensor for the $H \parallel y$ configuration can be expressed as a function of α and $\omega_z\tau$ (for simplicity we omit the index z),

$$\rho^{\text{open}} = \rho_0 \begin{pmatrix} \frac{\alpha - (\omega\tau)^2}{g_1 + (\omega\tau)^2} & 0 & \omega\tau \frac{\alpha - (\omega\tau)^2}{g_2 + (\omega\tau)^2} \\ 0 & 1 & 0 \\ -\omega\tau \frac{\alpha - (\omega\tau)^2}{g_2 + (\omega\tau)^2} & 0 & \alpha \frac{\alpha - (\omega\tau)^2}{g_3 + (\omega\tau)^2} \end{pmatrix}. \quad (5)$$

In this configuration the current is perpendicular to the applied magnetic field and it can be along the \hat{x} or \hat{z} directions. Instead, for the $H \parallel z$ case, the resistivity tensor is the one expected for closed orbits;

$$\rho^{\text{closed}} = \rho'_0 \begin{pmatrix} 1 & \omega\tau & 0 \\ -\omega\tau & 1 & 0 \\ 0 & 0 & g_4 \end{pmatrix}. \quad (6)$$

Both tensors are antisymmetric and follow Onsager's relations. We group most of the constants in ρ_0 , while g_i are geometric factors that come from the FS integrals. The off diagonal elements of ρ^{open} and ρ^{closed} are the so called ordinary Hall resistivity, which is obtained in the frame of semiclassical theory.

For the case $H \parallel y$, we plot in Fig. 2 the ordinary Hall resistivity ρ_{xz}^{open} and the MR (inset) for different values of the parameter g_2/α . The ordinary Hall has a root when $\omega_y\tau = 1$ or equivalently $\omega_z\tau = \sqrt{\alpha}$, and then it changes the sign, which can be interpreted as a switch of carrier type, from holelike to electronlike. For all values of g_2/α , the ordinary Hall ρ_{xz}^{open}

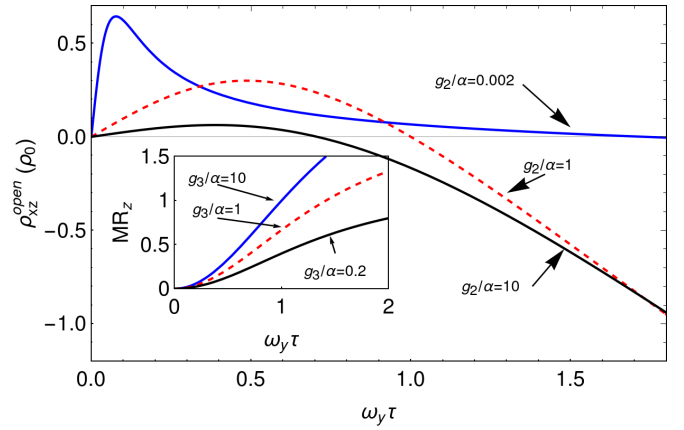


FIG. 2. Curves corresponding to Eq. (5) as a function of $\Omega\tau$, where $H \parallel y$ axis (see Fig. 1). Ordinary Hall is given in units of ρ_0 and the magnetoresistance (inset) assumes the current in z direction. The different curves correspond to values of g_2/α with $\alpha = \frac{m_z}{m_x}$ and g_2 is a geometric factor that comes from the integration of Eq. (1).

presents a mixed behavior with applied magnetic field. For values of $\omega\tau < 1$, the Hall resistivity is positive and reaches a maximum value that depends on α . If $g_2/\alpha = 1$, then the maximum of ρ_{Hall} is reached for $\omega\tau \approx 0.5$, higher values of g_2/α displace the maximum to zero, and for smaller values the maximum approaches 1. The MR defined as $|\rho_{ii}(\mathbf{H}) - \rho_{ii}(0)|/|\rho_{ii}(0)|$ saturates for values of $\omega\tau$ where the RTA and the low field condition are no longer valid ($\omega\tau \gg 1$). In all the cases of g_3/α , the MR presents a quadraticlike behavior for $\omega\tau < 1$, as expected for open orbits.

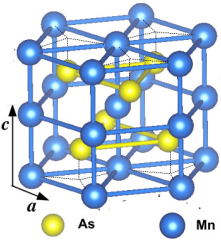
The goniopolar behavior is manifested by comparing Eqs. (5) and (6), where a different magnetotransport behavior should be expected for this kind of FS. When the magnetic field is parallel to the y axis ($H \parallel y$), the ordinary Hall resistivity as a function of the applied magnetic field presents a nonmonotonic behavior, having a positive slope for lower $\omega_z\tau$ values and a negative slope for higher ones. Instead, when the magnetic field is parallel to the z axis ($H \parallel z$), the ordinary Hall resistivity presents a linear behavior with increasing field.

Nevertheless, the present analysis is for a single band FS which is simply connected. In the case of multiband transport, the effects that come from other FS sheets should be taken into account in order to reproduce the experimental results. However, the curves obtained for the hyperboloid model, especially for $g_2/\alpha \approx 1$, present the same behavior with applied magnetic fields as our experimental measurements to be shown in Sec. III B done on MnAs/GaAs epilayers, and similar to the ones that were reported in [10,11]. This led us to study the FS of MnAs.

III. MnAs COMPOUND

MnAs is ferromagnetic at room temperature and can be grown by molecular beam epitaxy (MBE) onto several technologically relevant semiconductors as GaAs and Si [15,18,19]. Its ferromagnetic α phase crystallizes in the hexagonal NiAs structure with space group $P63/mmc$ for temperatures lower than 300 K as shown in Table I [20]. The magnetic easy axis lies in the hexagonal plane ab and the hard direction is parallel

TABLE I. Relations among components of the resistivity for the $P63/mmc$ space structure. The figure shows the atomic arrangements as well as the lattice parameters.

Structure	Direction	Relation
	$\mathbf{H} \parallel c$ axis ($H \parallel z$)	$\rho_{xz} = \rho_{yz} = 0$ $\rho_{xy}(H) = -\rho_{yx}(-H)$
	$\mathbf{H} \parallel ab$ plane ($H \parallel y$)	$\rho_{xy} = 0; \rho_{xx} = \rho_{yy}$ $\rho_{xz}(H) = -\rho_{zx}(-H)$

to the c axis. Table I shows a scheme of the structure as well as the relations between components of the resistivity tensor due to the symmetries of the crystal structure.

A. Electronic properties

Following the early suggestion in Ref. [11], that the features of the FS are responsible for the behavior of the Hall resistivity in the presence of an applied magnetic field, we obtain the FS by *ab initio* band-structure calculations by means of the QUANTUM ESPRESSO code (QE) [21]. We use the well known generalized gradient approximation with Perdew-Burke-Ernzerhof (GGA-PBE) for the exchange correlation potential with 8000 points in the first Brillouin zone

in the reciprocal space. Since we want to describe the system for magnetic fields for which the magnetization is saturated in a specific crystal direction, our calculations take into account the spin-orbit coupling (SOC) as implemented in the QE code and use fully relativistic pseudopotentials for both the Mn and the As atoms [21].

Our *ab initio* calculations are restricted to the two alignments consistent with the experimental geometries determined by the substrate orientation (Sec. III B). Table I shows the two different orientations of the magnetic field that can be aligned with the c axis of the crystal structure ($H \parallel z$ case) or with the b axis ($H \parallel y$ case).

We found four bands crossing the Fermi level which lead to a FS built by many sheets. The calculated energy isosurface in the reciprocal space, for each band that crosses the Fermi level in the $H \parallel y$ case, are presented in Figs. 3(a)–3(d). Our results indicate that the direction of the magnetic moments do not affect the shape of the FSs. Nevertheless, one situation has to be mentioned: the FS in Fig. 3(a) has a small ellipsoid around Γ and a “flat flower” close to the Δ symmetric point. This band is affected by the SOC in the $H \parallel z$ case, producing a small splitting around the Γ point, leaving the Fermi level inside the gap. As a consequence the ellipsoidal sheet around Γ disappears for the $H \parallel z$ configuration. The area of this ellipsoid is small compared with other FS sheets and, consequently, its contribution at low temperatures to the MR and to the Hall conductivity is negligible.

The surface shown in Fig. 3(b) has two not-connected sheets, where the red part indicates the side of the surface

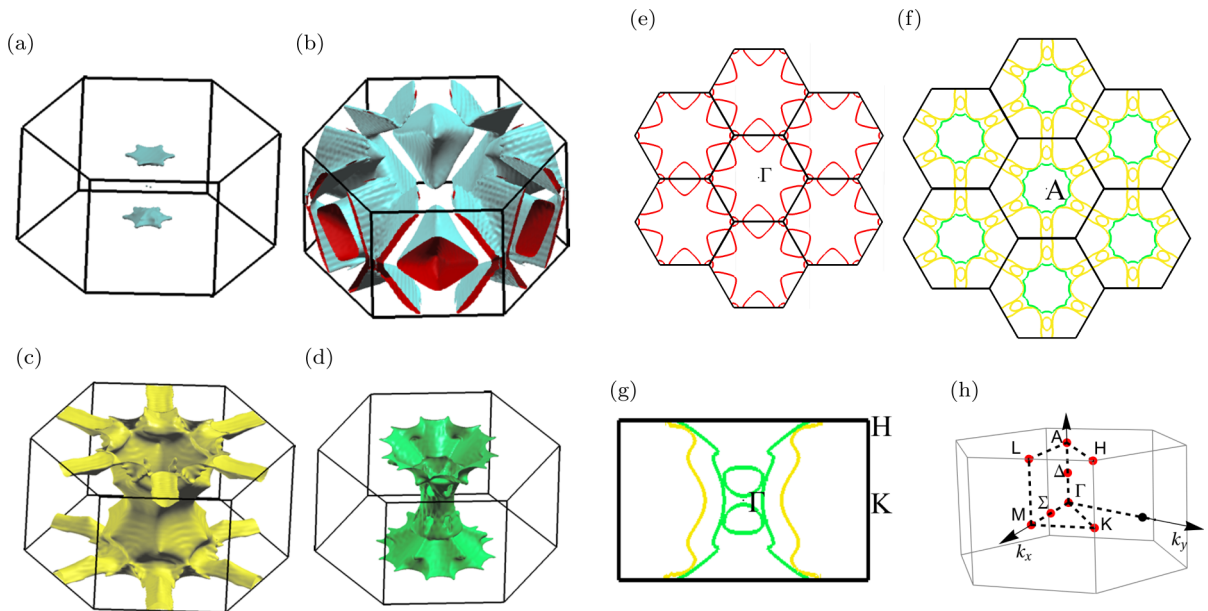


FIG. 3. (a)–(d) Fermi surfaces obtained for $H \parallel z$ case. (a) There is a flat flower around the Δ point, while the ellipsoid around Γ is not appreciated on this scale. (b) For this band, the FS is not simply connected and has two independent sheets, one showing a “nut” shape in the extended zone, and the other one presenting an “X” shape centered at the K point that is folded on itself and does not reach the top and bottom boundaries. Panels (c) and (d) are FS having hyperboloidlike shapes. (e) Cross section of the band plotted in (b) along an extended plane that contains the Γ - K - M points; only closed orbits are present. (f) Cross section of the band plotted in (c) yellow and (c) green in an extended plane that contains points along A - L - H . The connections among yellow lines indicate that this surface holds open orbits in directions perpendicular to the c axis. (g) Cross section of the bands plotted in (b) and (c) in a plane that contains the Γ - H - K points; it presents open orbits along the c axis and a curvature that can be extrapolated to a hyperboloidlike surface cut. (h) First Brillouin zone and its symmetric points used as reference.

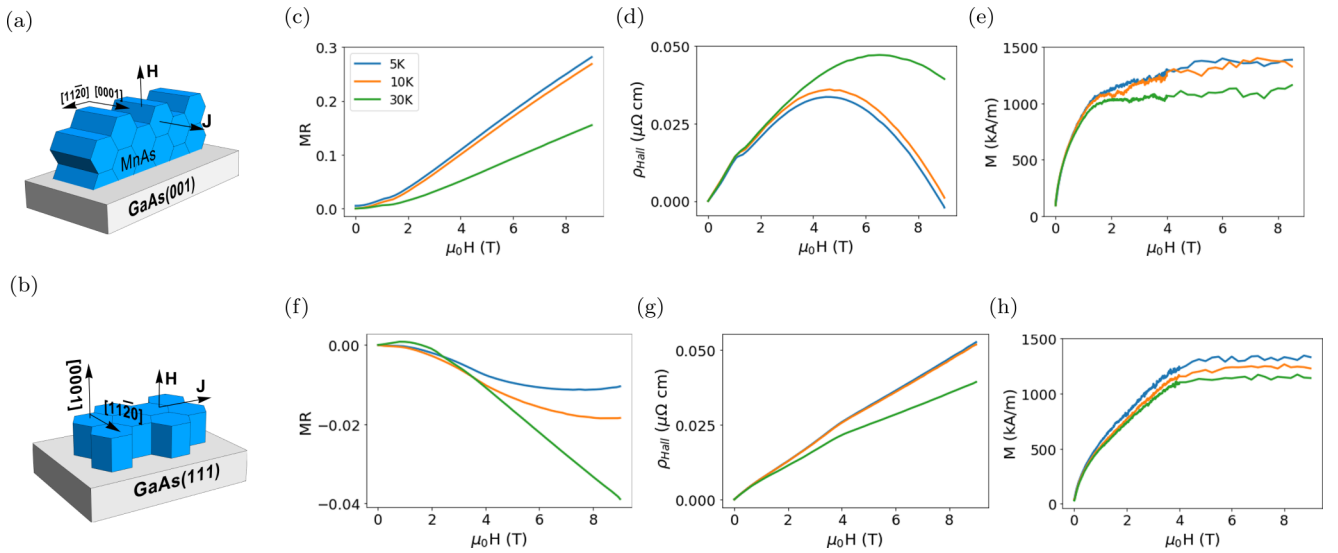


FIG. 4. Magnetotransport measurements in MnAs/GaAs(001) ($H \parallel y$), upper row, and MnAs/GaAs(111) ($H \parallel z$), lower row, showing magnetoresistance (c),(f), Hall resistivity (d),(g), and magnetization (e),(h) for both epitaxies as a function of the applied magnetic field and temperature. The MR is positive and does not saturate along (c), while it is negative and saturates for low temperatures in (f). The Hall resistivity (d) shows a change in the carrier type manifested in the change of slope at $\sim 5\text{--}7$ T, depending on T , that is not observed in (g); it displays a linear behavior. The shoulder observed at ~ 1.5 T in (d) and at ~ 4 T in (g) is related to the saturation of the magnetization in (e) and (h) at the corresponding fields, respectively.

facing the occupied states. One of them has the shape of a nut when plotted in an extended BZ, but does not connect opposite borders, thus only closed orbits are allowed. The other one has an X shape built by a sheet folded on itself, but it does not reach the top and bottom Brillouin zone borders. Also, it makes a negligible contribution to the conductivity tensor, since the normal vector $d\mathbf{S}$ has opposite directions for nearby points in reciprocal space. To visualize one possible orbit on this surface, we plot in Fig. 3(e) the cross section in the repeated zone of a plane perpendicular to the k_z axis that contains the Γ point; it is clear that there is no possibility of holding open orbits.

The FSs of interest are those shown in Figs. 3(c) and 3(d). Both surfaces are hyperboloidlike along the k_z axis, which is parallel to the c -crystal axis. Now the association of these surfaces with the model presented in Sec. II becomes clear: when the magnetization is parallel to the c axis, it is related to the case where the magnetic field is parallel to the z axis of the hyperboloid model ($H \parallel z$ configuration). On the other hand, when magnetization is parallel to the hexagonal planes, it relates to the $H \parallel y$ configuration. In Fig. 3(f) we present the cross section of the bands plotted in Figs. 3(c) and 3(d) at the repeated zone in a plane perpendicular to k_z axis that contains the A point. Interestingly, a path that contains open orbits in a direction perpendicular to the k_z axis is observed.

The last two mentioned FSs have hyperboloidlike surface, which, as we describe in the previous section, could lead to a goniopolar magnetotransport behavior.

B. Magnetotransport measurements

The MnAs samples were epitaxially grown on GaAs(001) and GaAs(111) substrates [22,23], as depicted in Fig. 4, first column. These samples allow us to study the magnetotrans-

port phenomena in two different MnAs-crystal orientations, where the applied magnetic field is parallel to the plane of the hexagon ($H \parallel y$) and the other one where the applied field is perpendicular to it ($H \parallel z$), as indicated in Fig. 4. Magnetotransport data and magnetization measurements as a function of external magnetic field and temperature were done in a physical property measurement system (PPMS) using the Van der Pauw electric contact configuration [24].

Results on the MnAs/GaAs(001) sample ($H \parallel y$) are displayed in the upper row of Fig. 4. The MR presented in Fig. 4(c) is positive with positive slope for all temperatures, having a quasiparabolic behavior, and does not saturate for the maximum applied field of 9 T.

The Hall resistivity dependence with applied magnetic field (d) has a nonmonotonic behavior, showing a change in the slope around $\sim 5\text{--}7$ T, that depends on the temperature. This behavior has already been reported in Refs. [10,11] and was ascribed to a change in the type of carriers. Our model anticipates this change in carrier types with applied magnetic field when FSs present hyperboloid shapes as the one obtained by density functional theory calculations in the previous section. The magnetization vs field shown in Fig. 4(e) rises until ~ 1 T and gradually saturates upon increasing the magnetic field. The noticeable shoulder at ~ 1 T in the Hall resistivity is related to the magnetization saturation at this field value, and indicates the saturation of the anomalous Hall effect [25].

For the MnAs/GaAs(111) sample ($H \parallel z$ case), the MR presented in Fig. 4(f) has negative values and negative slope, and saturates for increasing applied magnetic field for the 5- and 10-K curves. Instead, for 30 K the saturation is not reached for the maximum applied field of 9 T. This saturation observed in the low field regime indicates dominance of closed orbits in momentum space at low temperatures. The Hall resistivity for the MnAs/GaAs(111) sample displayed

in Fig. 4(g) has a linear behavior with increasing magnetic field, as expected for the hyperboloidlike FS with magnetic field parallel to symmetry axis. There is a subtle change of slope at 4 T, which is the same field where the magnetization saturates as shown in Fig. 4(h), suggesting the saturation of the anomalous Hall contribution to the Hall resistivity.

MBE growth ensures an excellent crystal quality as well as sharp interfaces between the MnAs layer and the GaAs substrate [13], allowing us to rule out any significant role of the impurities at low temperatures. Also, possible magnetic domains disappear when magnetic saturation is reached.

To summarize the experimental results for different crystalline orientations, MnAs/GaAs(001) shows a change of carrier type with increasing magnetic field, but for MnAs/GaAs(111) the carrier type is conserved. This means that the ordinary Hall behavior with magnetic field is in agreement with the model discussed in Sec. II for FSs like the ones presented in Sec. III A. This is the main issue we addressed in this work.

IV. DISCUSSION

In order to reproduce the experimental results with the modeled FS, it is necessary to take into account that the Hall resistivity measurements include two contributions: the ordinary and the anomalous Hall, respectively. They are related to the total Hall resistivity by [25,26]

$$\rho_{\text{Hall}}(H) = \rho_{\text{ord}}(H) + R_A \mu_0 M(H, T), \quad (7)$$

where H and M are the applied magnetic field and magnetization of the sample in the out of plane direction, respectively. ρ_{Hall} is the measured Hall resistivity, R_A is the anomalous Hall coefficient, and ρ_{ord} is the ordinary Hall contribution, which is obtained from the nondiagonal elements of the Eqs. (5) and (6).

The Hall resistivity in MnAs/GaAs(111) presents a linear behavior with applied magnetic field [Fig. 4(g)]. This result is expected as we proved that in this configuration the possible orbits in reciprocal space are closed. From Eq. (6) we obtain a linear behavior for this case, where $\rho_{\text{ord}} = \rho_0 H$. Instead, we predicted open orbits for the sample MnAs/GaAs(001), and our experimental results on Hall resistivity show a nonlinear behavior with the applied magnetic field. For this last case, we use $\rho_{x,z}^{\text{open}}$ from Eq. (5) as ρ_{ord} in Eq. (7) to reproduce the experimental results.

The agreement between the model and experimental Hall measurements for MnAs/GaAs (001) is shown in Fig. 5. The fit yields a $g_2/\alpha \approx 2.10$, which is comparable with the 4.09 and 1.41 values obtained for the FS of Figs. 3(d) and 3(c) respectively, by using Eq. (4). Finally, the coefficient $R_A = 0.1 \frac{\mu\Omega \text{ cm}}{\text{T}}$ is of the same order of magnitude of similar metallic systems [27,28].

The results from the electronic structure calculation presented in Sec. III A show a multiband contribution to the electron transport with four bands crossing the Fermi level. The band presented in Fig. 3(a) has a negligible number of states compared with the other bands, which diminishes its contribution to conductivity. In addition, the band presented in Fig. 3(b) is not a simply connected surface and it is made of two sheets that contribute with close orbits. In that case,

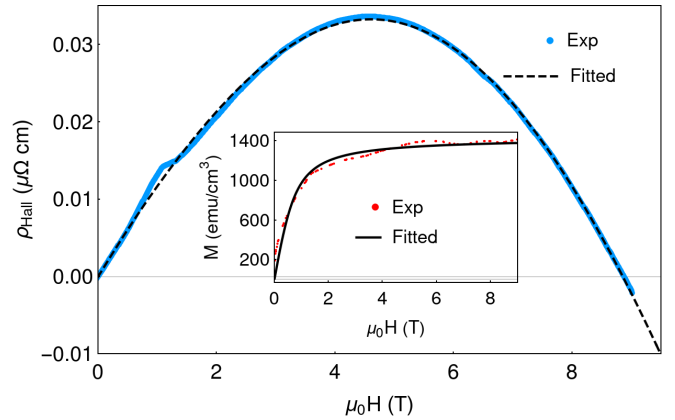


FIG. 5. Experimental measurement at 5 K of the Hall resistivity for sample MnAs/GaAs(001) fitted using Eq. (7), where $\rho_{\text{ord}} = \rho_{x,z}^{\text{open}}$. At the inset the magnetization is fitted by a Langevin function.

one of the sheets is folded on itself and its contribution to the conductivity is also negligible. The remaining two bands have a hyperboloidlike shape along the z axis in reciprocal space and they are the main contribution to the magnetoresistance dependence with magnetic field at low temperatures.

Another scenario that could produce a change in the sign of the Hall resistivity is the Sondheimer oscillations [29]. This effect produces oscillations that simultaneously affect the magnetoresistance and the Hall resistivity. It is observed in aluminum thin films [30], which has similar FS with a nutlike shape in the extended BZ as the one presented in Fig. 3(b). However, our measurements of the MR [Figs. 4(c)–4(f)] do not show any oscillation even for applied magnetic fields up to 14 T [10,11]. Finally, the trend of the Hall resistance remains unaltered after it changes its sign.

V. CONCLUSION

The experimental data evidence the different behavior of the charge carriers depending on the crystal direction. For MnAs/GaAs(001) ($H \parallel y_0$ configuration), the carrier polarity changes when the system goes from a low field state ($\omega\tau < 1$) to a high field state ($\omega\tau > 1$), while this change of carrier polarity cannot be observed in MnAs/GaAs(111) ($H \parallel z$ configuration). We modeled this behavior using the specific topology of the dominant FSs sheets with a hyperboloid shape, obtaining a good agreement with measurements. However, further studies should be done to classify this material as goniopolar. Measurements of the Seebeck effect univocally determine this classification because this effect is dominated by the FS shape. We believe our study provides guidelines to study the magnetotransport properties in a broad range of materials with similar FSs.

ACKNOWLEDGMENTS

Samples were grown by E. Islam and M. Akabori at Center for Nano Materials and Technology (CNMT), Japan Advanced Institute of Science and Technology (JAIST), 1-1 Asahidai, Nomi, Ishikawa 923-1292, Japan. We acknowledge D. P. Daroca, C. Gourdon, L. Thevenard,

D. Hrabovsky, and Y. Klein for the valuable discussions and their assistance in the magnetotransport measurements at the “Plateforme de mesures physiques a basse temperature” at Sorbonne Université. Complementary XRD measurements were done by D. Vega at the Condensed

Matter Department of CAC-CNEA. This work was supported by CONICET (Grant No. PIP 11220115-0100213 CO), ANPCyT (Grant No. PICT-2016-0867), and LIFAN (Laboratoire International Franco Argentin en Nanosciences) collaborations.

- [1] A. B. Pippard, Experimental analysis of the electronic structure of metals, *Rep. Prog. Phys.* **23**, 176 (1960).
- [2] M. K. M. Lifshitz and M. I. Azbel, On the theory of Galvanomagnetic Effects in metals, *Sov. Phys. - JETP* **3**, 143 (1956).
- [3] R. N. Gurzhi and A. I. Kopeliovich, Galvanomagnetic properties of metals with closed Fermi surfaces at low temperatures, *Sov. Phys. - JETP* **40**, 1144 (1975).
- [4] N. Gurzhi and I. Kopeliovich, Galvanomagnetic properties of metals with open Fermi surfaces, *Sov. Phys. - JETP* **44**, 334 (1977).
- [5] S. P. Novikov, R. De Leo, I. A. Dynnikov, and A. Y. Maltsev, Theory of dynamical systems and transport phenomena in normal metals, *J. Exp. Theor. Phys.* **129**, 710 (2019).
- [6] B. He, Y. Wang, M. Q. Arguilla, N. D. Cultrara, M. R. Scudder, J. E. Goldberger, W. Windl, and J. P. Heremans, The Fermi surface geometrical origin of axis-dependent conduction polarity in layered materials, *Nat. Mater.* **18**, 568 (2019).
- [7] Y. Wang, K. G. Koster, A. M. Ochs, M. R. Scudder, J. P. Heremans, W. Windl, and J. E. Goldberger, The chemical design principles for axis-dependent conduction polarity, *J. Am. Chem. Soc.* **142**, 2812 (2020).
- [8] S. K. Radha and W. R. L. Lambrecht, Topological band structure transitions and goniopolar transport in honeycomb antimonene as a function of buckling, *Phys. Rev. B* **101**, 235111 (2020).
- [9] S. Zhang, Q. Wu, Y. Liu, and O. V. Yazyev, Magnetoresistance from Fermi surface topology, *Phys. Rev. B* **99**, 035142 (2019).
- [10] J. J. Berry, S. J. Potashnik, S. H. Chun, K. C. Ku, P. Schiffer, and N. Samarth, Two-carrier transport in epitaxially grown MnAs, *Phys. Rev. B* **64**, 052408 (2001).
- [11] K.-J. Friedland, M. Kästner, and L. Däweritz, Ordinary Hall effect in MBE-grown MnAs films grown on GaAs(001) and GaAs(111)B, *Phys. Rev. B* **67**, 113301 (2003).
- [12] L. Berger, Hall effect of a compensated magnetic metal proportional to MB2 in the high-field limit, *Phys. Rev.* **177**, 790 (1969).
- [13] L. Däweritz, F. Schippan, A. Trampert, M. Kästner, G. Behme, Z. Wang, M. Moreno, P. Schützendübe, and K. Ploog, MBE growth, structure and magnetic properties of MnAs on GaAs on a microscopic scale, *J. Cryst. Growth* **227-228**, 834 (2001).
- [14] M. Ramsteiner, H. Y. Hao, A. Kawaharazuka, H. J. Zhu, M. Kästner, R. Hey, L. Däweritz, H. T. Grahn, and K. H. Ploog, Electrical spin injection from ferromagnetic MnAs metal layers into GaAs, *Phys. Rev. B* **66**, 081304(R) (2002).
- [15] N. Mattoso, M. Eddrief, J. Varalda, A. Ouerghi, D. Demaille, V. H. Etgens, and Y. Garreau, Enhancement of critical temperature and phases coexistence mediated by strain in MnAs epilayers grown on GaAs(111)B, *Phys. Rev. B* **70**, 115324 (2004).
- [16] N. W. Ashcroft and N. D. Mermin, *Solid State Physics* (Holt, Rinehart and Winston, New York, 1976).
- [17] Y. C. Akgöz and G. A. Saunders, Space-time symmetry restrictions on the form of transport tensors. II. Thermomagnetic effects, *J. Phys. C: Solid State Phys.* **8**, 2962 (1975).
- [18] M. Tanaka, Ferromagnet (MnAs)/III V semiconductor hybrid structures, *Semicond. Sci. Technol.* **17**, 327 (2002).
- [19] M. Tanaka, J. P. Harbison, M. C. Park, Y. S. Park, T. Shin, and G. M. Rothberg, Epitaxial orientation and magnetic properties of MnAs thin films grown on (001) GaAs: Template effects, *Appl. Phys. Lett.* **65**, 1964 (1994).
- [20] I. Rungger and S. Sanvito, *Ab initio* study of the magnetostructural properties of MnAs, *Phys. Rev. B* **74**, 024429 (2006).
- [21] P. Giannozzi *et al.*, Advanced capabilities for materials modelling with Quantum ESPRESSO, *J. Phys.: Condens. Matter* **29**, 465901 (2017).
- [22] M. E. Islam and M. Akabori, Growth and magnetic properties of MnAs/InAs hybrid structure on GaAs(111)B, *J. Cryst. Growth* **463**, 86 (2017).
- [23] M. E. Islam and M. Akabori, In-plane isotropic magnetic and electrical properties of MnAs/InAs/GaAs(111)B hybrid structure, *Physica B (Amsterdam, Neth.)* **532**, 95 (2018), special issue on Frontiers in Materials Science: Condensed Matters.
- [24] L. J. van der Pauw, A method of measuring specific resistivity and Hall effect of discs of arbitrary shape, *Philips Res. Rep.* **13**, 1 (1958).
- [25] E. M. Pugh and T. W. Lippert, Hall e.m.f. and Intensity of Magnetization, *Phys. Rev.* **42**, 709 (1932).
- [26] S. H. Chun, Y. S. Kim, H. K. Choi, I. T. Jeong, W. O. Lee, K. S. Suh, Y. S. Oh, K. H. Kim, Z. G. Khim, J. C. Woo, and Y. D. Park, Interplay Between Carrier and Impurity Concentrations in Annealed Ga1-xMnxAs: Intrinsic Anomalous Hall Effect, *Phys. Rev. Lett.* **98**, 026601 (2007).
- [27] Y. Yang, Z. Luo, H. Wu, Y. Xu, R. W. Li, S. J. Pennycook, S. Zhang, and Y. Wu, Anomalous Hall magnetoresistance in a ferromagnet, *Nat. Commun.* **9**, 1 (2018).
- [28] C. Helman, A. Camjayi, E. Islam, M. Akabori, L. Thevenard, C. Gourdon, and M. Tortarolo, Anomalous Hall effect in MnAs: Intrinsic contribution due to Berry curvature, *Phys. Rev. B* **103**, 134408 (2021).
- [29] E. H. Sondheimer, The Influence of a transverse magnetic field on the conductivity of thin metallic films, *Phys. Rev.* **80**, 401 (1950).
- [30] K. Fjørsvoll and I. Holwech, Sondheimer oscillations in the Hall effect of aluminium, *Philos. Mag.* **10**, 921 (1964).